Role of interface structure and chemistry in resistive switching of NiO nanocrystals on $SrTiO_3$

Xuan Cheng,[1] Jivika Sullaphen,[1] Matthew Weyland,[2] Hongwei Liu,[3] and Nagarajan Valanoor[1]
[1]*School of Materials Science and Engineering, University of New South Wales, Sydney NSW 2052, Australia*
[2]*Department of Materials Engineering and Monash Centre for Electron Microscopy, Monash University, Melbourne VIC 3800, Australia*
[3]*Australian Centre for Microscopy and Microanalysis, University of Sydney, Sydney NSW 2006, Australia*

(Received 7 November 2013; accepted 13 March 2014; published online 27 March 2014)

Nickel oxide (NiO) nanocrystals epitaxially grown on (001) strontium titanate ($SrTiO_3$) single crystal substrates were characterized to investigate interface morphology and chemistry. Aberration corrected high angle annular dark field scanning transmission electron microscopy reveals the interface between the NiO nanocrystals and the underlying $SrTiO_3$ substrate to be rough, irregular, and have a lower average atomic number than the substrate or the nanocrystal. Energy dispersive x-ray spectroscopy and electron energy loss spectroscopy confirm both chemical disorder and a shift of the energy of the Ti $L_{2,3}$ peaks. Analysis of the O *K* edge profiles in conjunction with this shift, implies the presence of oxygen vacancies at the interface. This sheds light into the origin of the previously postulated minority carriers' model to explain resistive switching in NiO [J. Sullaphen, K. Bogle, X. Cheng, J. M. Gregg, and N. Valanoor, Appl. Phys. Lett. **100**, 203115 (2012)]. [http://dx.doi.org/10.1063/1.4869457]

Nickel oxide (NiO) has been widely investigated for its optical,[2] (anti-) ferromagnetic,[3,4] and electrochromic properties.[5–7] It was recently found to have resistive switching (RS) properties, switching from a high resistance (OFF) state to a low resistive (ON) state (and back to OFF) by successive application of electric fields of opposite polarity.[8] In addition, its fast switching speeds and low energy consumption[9] makes NiO a viable candidate for next generation resistive random access memories (RRAMs). The demand for high-density memories has concentrated on RS materials with scalable dimensions, such as ultra-thin films,[10,11] nanowires,[12,13] and nanocrystals.[1] Consequently, many of the RS experiments have been performed on nanoscale NiO.[14–18] This scaling brings about enhanced interfacial chemistry effects that dominate RS. Changes to the chemical environment at the electrode interface have been reported to drive metal-oxide-metal (MOM) sandwich device performance.[19–22] For NiO, it has been proposed that an oxygen rich layer at the anode interface, controls the threshold switching of Pt-NiO-Pt system.[23]

The presence of point and line defects,[24] composition inhomogeneity,[25] and atomic interdiffusion[26] at interfaces have been shown to have a significant impact on device properties. As a consequence, interface characterization plays an important role in understanding the RS mechanisms observed for different nanoscaled transition metal oxides. In general, it can be said that detailed interface characterization is necessary for any nanoelectronic device that is based on metal oxides. Previously, we proposed an interface-mediated RS mechanism for epitaxial NiO nanocrystals grown on niobium doped strontium titanate (Nb: $SrTiO_3$) substrate.[1] The mechanism put forth was the redistribution of the minority carriers caused by oxygen vacancies under an applied electric field. However, direct evidence for the presence of oxygen vacancies at the interface in the first place

and their effects on the local chemistry of the interfacial structure was yet to be experimentally confirmed.

Here we apply scanning transmission electron microscopy (STEM) to carry out a direct investigation of the interfacial structure and chemistry in epitaxial NiO nanocrystals grown on (001) single crystalline strontium titanate ($SrTiO_3$) substrates. The interface, between the nanocrystal and the underlying substrate, is found to have chemical disorder and an irregular morphology. Electron energy loss spectroscopy (EELS) reveals a shift in the Ti $L_{2,3}$ peak position accompanied by dramatic peak intensity reduction, indicating a lower valance state for Ti at the interface. In addition, the O *K* edge at the interface plateaus out with energy loss increases, suggesting a breaking of long-range order.[27,28] By combining both Ti and O EELS results, oxygen vacancies are confirmed to be located at the NiO-$SrTiO_3$ interface. R × A measurements suggest that the interface chemistry should play a significant role in driving RS in NiO nanocrystals. These experimental results shed insight into how and where charge carriers could stem form, in the minority carrier model previously used to explain the RS mechanism in NiO nanocrystals.[1]

Pulsed laser deposition (PLD) with a phase separation approach was used to deposit NiO nanocrystals on a (001) $SrTiO_3$ single crystalline substrate.[29] Survey TEM images and selected area electron diffraction (SAED) patterns were acquired at 200 kV on a Philips CM200 FEG. High angle annular dark field (HAADF) STEM was carried out on a dual Cs corrected (probe and image) FEI Titan^3 80–300 FEGTEM operated at 200 kV. An illumination semi-angle of 18 mrad was used, corresponding to a probe size of ∼0.12 nm, and an inner collection semi-angle of 63 mrad. All the samples were tilted to the [110] zone axis for imaging. It was found that the NiO and NiO-$SrTiO_3$ interface were highly susceptible to beam damage at 200 kV. As such chemical analysis by energy dispersive X-ray spectroscopy (EDS) and EEL spectrum imaging (SI) were carried out at 80 kV where damage rates were manageable, if not negligible. (The EELS and EDS were carried out using a Gatan GIF Tridiem and an EDAX Genesis Si(Li) detector, respectively). To maximize current and collected signal STEM mode EELS mapping was operated with a convergence angle of 22 or 26 mrad (in separate experiments), to give an aberration limited probe size of >0.2 nm. The camera length was tuned to give a HAADF collection angle of 77–170 mrad and EELS collection angle of 38 mrad. Processing of EELS and EDX SI's were carried out in IDL V8.2.

Figure 1(a) shows the overall morphology of typical NiO nanocrystals. The atomic force microscope (AFM) surface profile, Figure 1(a), shows the morphology of the well-dispersed NiO nanocrystals to be both rectangular and square-based pyramids. The cross-sectional specimens shown in Figure 1(b) reveal them to be predominantly hut-shaped. The origin of this shape dependence can be found in Ref. 30. The TEM image in Figure 1(c) reveals distinct facets that bound the nanocrystal. These facets are indexed through the SAED pattern (Figure 1(c) inset), which indicates that the facets are planes that belong to {111} and {113} families. Furthermore, distinct diffraction spots in the SAED confirm the single crystalline nature of the NiO nanocrystal.

The HAADF-STEM image, Figure 1(d), shows the interface between the NiO nanocrystal and the $SrTiO_3$ substrate is both non-flat and of lower average atomic number than either the substrate or the nanocrystal (a higher magnification HAADF-STEM image along with the possible structure model is presented in Fig. S1 of the supplementary material[31]). Critically, we find no misfit dislocations despite the relatively large (7% compressive) lattice misfit strain. The role of this interface is discussed briefly towards the end. This drop in atomic number can be attributable to a change in projected thickness, chemistry, or the presence of vacancy defects. A fourth option, dechanneling due to strain, is ruled, as there is no significant contrast change upon changing the HAADF collection angle. As HAADF-STEM can only indicate the average projected atomic number rather than the exact chemistry, or oxidation state, of the interface, spatially resolved chemical analysis by EELS and/or EDX was required.

Figure 2(a) shows the results of EELS chemical mapping of a NiO-$SrTiO_3$ interface. The maps suggest that there is mixing of Ni and Ti near the interface. The lack of a sharp interface in the O *K* map, despite the strong difference in O density and bonding between NiO and $SrTiO_3$, suggest a third O environment at the interface. It is however somewhat difficult to rule out thickness effects on the total signal.

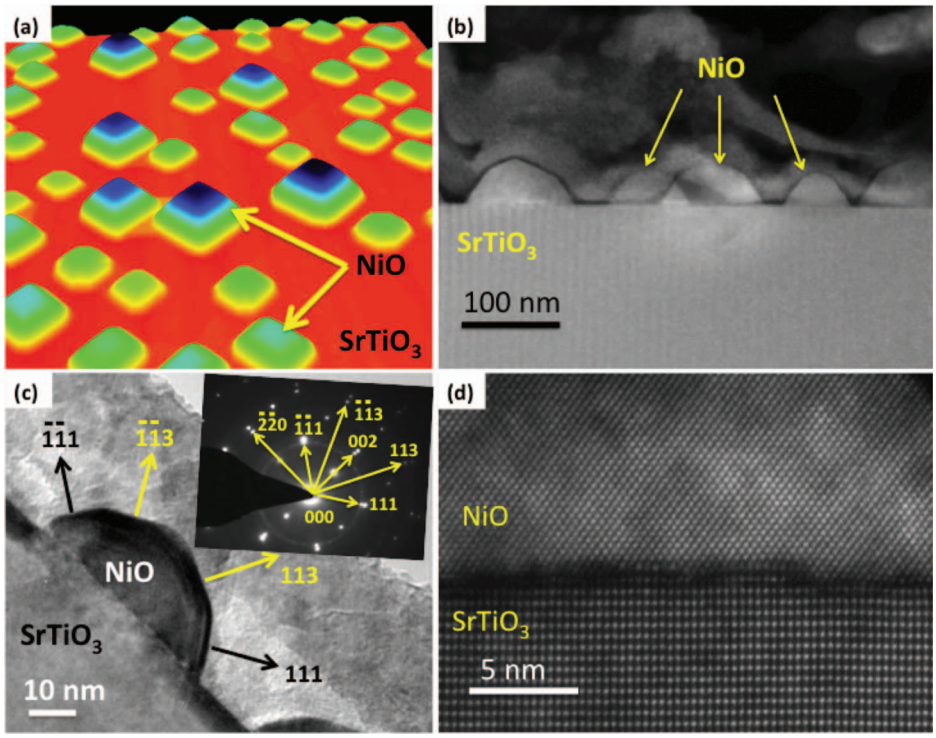

FIG. 1. (a) Three-dimensional atomic force microscope (AFM) image shows morphology of the NiO nanocrystals grown on the $SrTiO_3$ substrate. (b) High angle annular dark field (HAADF) scanning transmission electron microscope (STEM) image shows a cross-sectional specimen of NiO-$SrTiO_3$. (c) Bright field (BF) transmission electron microscope (TEM) image and selected area electron diffraction (SAED) pattern of the area (inset) show that the NiO nanocrystal is bound by {111} and {113} facets. (d) A HAADF-STEM image shows the rough interface with atomic resolution. The dark layer at the interface indicates a lower average atomic number than the nanocrystal or the substrate.

In order to reveal more detailed chemical information, EELS and EDS were simultaneously acquired from a line scan, with 0.5 nm per pixel, across the NiO-$SrTiO_3$ interface (marked as yellow arrow in Figure 2(b)). Line traces of the EELS and EDS results are shown in Figures 2(c) and 2(d). The dark layer at the interface, as indicated by white arrows in Figure 2(b), is the trough in the HAADF intensity plot. A more accurate width of the boundary between NiO and the $SrTiO_3$ substrate can be given by the full width at half maximum (FWHM) of the HAADF trough, which is approximately 0.5 nm. The probe size in EELS experiments were of the order of 0.3 nm, thus the artifacts caused by beam spreading will be very limited. Both EDS (Figure 2(c)) and EELS (Figure 2(d)) show penetration of Ti into the NiO nanocrystal. EDS also shows that Sr has spread across the interface along with Ti. Thus the EELS and EDS line scans provide clear evidence of chemical intermixing between NiO and $SrTiO_3$; more importantly, the location of the trough in the O *K* profile signifies the true interface between the nanocrystal and the substrate.

From the EELS line scan, 6 representative Ti $L_{2,3}$ edges (450–480 eV, shown in Figure 3) and 3 O *K* edges (520–560 eV) were extracted from selected points (point *a* to *f*, shown in Figures 2(b) and 2(d)) for further analysis. In perovskite materials, such as $SrTiO_3$ and $PbTiO_3$, the Ti white lines show L_3 and L_2 edges. These edges are due to crystal field splitting, arising from $2P^{3/2} \rightarrow 3d^{3/2}3d^{5/2}$ and $2p^{1/2} \rightarrow 3d^{3/2}$ transitions, respectively. Each Ti edge splits into two sub-edges t_{2g} and e_g related to the hybridization and ligand field strength of the Ti-O atomic interaction.[32] These $L_{2,3}$ edge splits can be observed from point *f* to point *e*, which implies that they are from $SrTiO_3$ substrate, as expected. However, the intensity of the Ti white lines decreases dramatically from point *e* to point *d*, leading to electronic states not as distinctly defined compared to $SrTiO_3$ when closer to the interface. This comes along with the significant reduction of the $L_{2,3}$ edges peak splitting, which reflects a weaker Ti-O hybridization and ligand strength. Furthermore, the final disappearance of Ti $L_{2,3}$ peaks

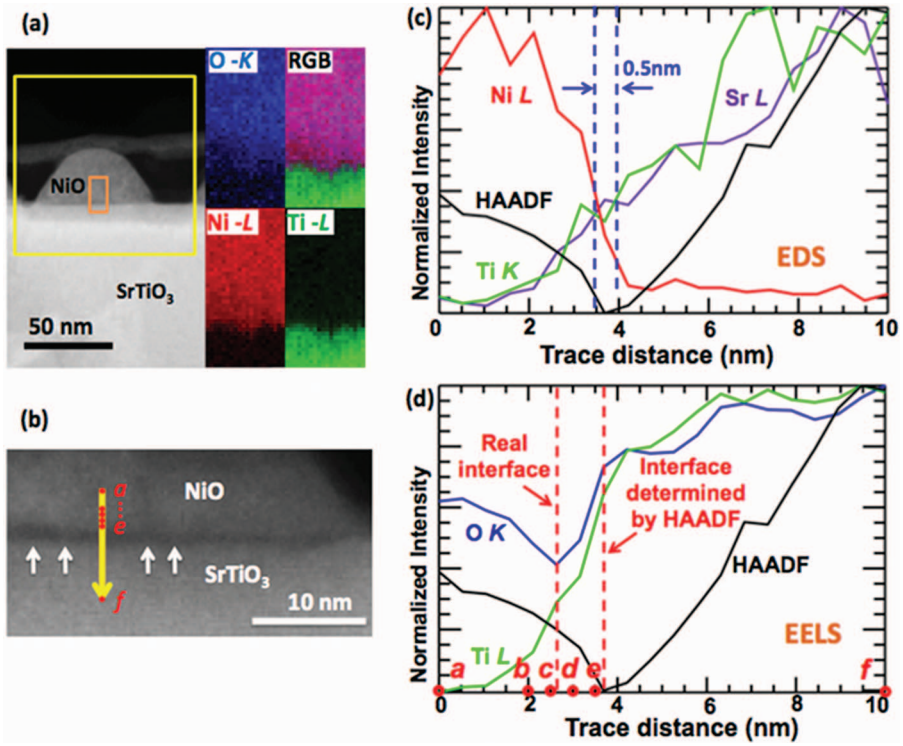

FIG. 2. (a) Electron energy loss spectrum (EELS) image (10 × 20 nm) of the interface (the orange rectangular and yellow square indicate the mapping and drift-correction area, respectively) reveals an oxygen deficient layer at the interface. The individual EELS maps are generated with intensities of Ni $L_{2,3}$, Ti $L_{2,3}$, and O K as red, green, and blue channels, respectively. The red green blue (RGB) image is produced with integration of all three intensities. (b) HAADF-STEM image of the interface indicates the location of the probe (yellow arrow). (c) Energy dispersive x-ray spectroscopy (EDS) line scans along the interface show Ti and Sr penetrate into the nanocrystal. (d) EELS line scans confirm the chemical intermixing at the interface and reveal the real location of the interface between NiO and $SrTiO_3$.

splitting suggests that the real interface is located between point *c* and *d*, rather than at the dark layer as shown in Figure 2(b). In other words, the chemical interface is about 1–2 nm above the dark layer and is located within the NiO nanocrystal. Moreover, from the $SrTiO_3$ substrate to the interfacial layer, $L_{2,3}$ edges shift slightly towards the lower energy loss, indicating a lower oxidation state of Ti (+4-δ) at the interface, which is lower than Ti in the $SrTiO_3$ substrate (+4).[27] This shift is more obvious from the Ti $L_{2,3}$ EEL spectrum image shown in Figure 3(b).

The results from the Ti $L_{2,3}$ edge analyses are further corroborated by analysis of oxygen O K spectra (shown in Figure 3(c)). Muller *et al.* have previously ascribed the fine changes in Ti $L_{2,3}$ EEL spectra and correspondingly alterations to the O K spectra are due to the presence of oxygen vacancies in $SrTiO_3$.[27] Here we present similar findings obtained in Ti $L_{2,3}$ edges and O K edges at the interface. While $SrTiO_3$ (point *f*) shows clear peak splitting γ_1 and γ_2, in the case of NiO (point *a*), there is no peak splitting observed from the prepeak of O K edge as the $2t_{2g}$ state of Ni is completely occupied.[33] Instead only one sharp peak (peak γ) is shown. Peak δ_1 and δ_2 are mapping the Ni 4sp bands and other bands with counter-ion character, which are related to the oxygen coordination. At the interface (point *d*), the O K edge shows a very ambiguous peak γ with a lower intensity than γ_1 and γ_2 peak in $SrTiO_3$ or γ peak in NiO. More remarkably, the edge plateaus out with energy loss increases and the peak δ disappears. These indicate a breaking of long range order and further suggest the presence of oxygen vacancies at the interface of NiO and $SrTiO_3$.[27,28]

There could be a number of factors contributing to the presence of oxygen vacancies. First, they could be inherent in the synthesis process as the samples are annealed in vacuum as a final step in order to achieve the desired morphology. Second, it has been recently predicted that in the perovskite $CaMnO_3$, point defects formation is a possible strain relaxation mechanism.[34] As seen

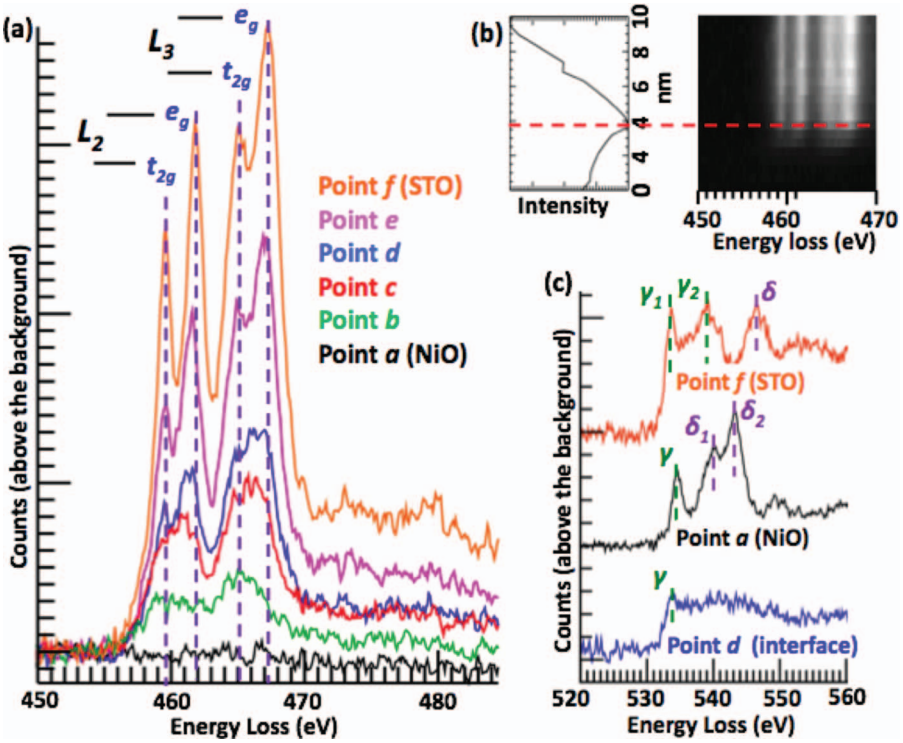

FIG. 3. (a) Ti *L* edges of the selected points (points *a* to point *f* as shown in Figure 2(b) and 2(d)) from EELS line scan. (b) ADF intensity plot and EEL spectrum image simultaneously acquired with EELS. (c) Simultaneously acquired O *K* edges from point *a*, *d*, and *f*.

in Fig. S1 of the supplementary material,[31] there were no distinct misfit dislocations observed at this interface. On the other hand we find that the strain between NiO and $SrTiO_3$ is accommodated by a long-range vacancy ordering, where the 13 unit cells of NiO are aligned with 14 unit cells of $SrTiO_3$.[35] This translates approximately to a 0.8% residual mismatch strain, which is significantly lower than the theoretical value. Finally, a redox reaction could be happening at the NiO-$SrTiO_3$ interface spontaneously due to the variation in the oxygen affinities for Ni vs. Ti (due to TiO_2 terminated parts of the substrate). The latter two possibilities are currently being investigated in further detail and form the basis of an upcoming study.[35]

Previously NiO thin films (polycrystalline) have been reported to carry a reservoir of oxygen ions that facilitates their RS mechanisms,[36] dependent on the formation and rupture of the conductive filaments (CFs) at a nanoscale level.[37] The formation of CFs is a behavior of defect generation, which can be affected by the crystallographic structure of the material. For polycrystalline materials, oxygen vacancies usually form plane defects or grain boundaries. Therefore, we probed further the possibility of the RS behavior being influenced by such defects at the interface. Following Kohlstedt *et al.*,[38] the independence of the R × A product of A implies that the RS is an interface dominated effect. Therefore R × A measurements were carried out (as shown in Fig. S2 of the supplementary material).[31] We show that the R_{on} × A (low resistance state) product is independent of the measured areas (for nanocrystals with heights ∼15–23 nm). In contrast it deviates for the largest area, which is for a nanocrystal that measured 23 nm in height. In this case, the nanocrystal is too high for any interface-driven effects as explained in our previous paper[1] and thus demonstrates weaker resistance modulation. Additionally, the current values for the pristine nanocrystal and high resistance state are almost similar (see Fig. S2 of the supplementary material[31]).

We highlight that similar RS has been found in $SrTiO_3$, in which the CFs are formed through dislocations.[39] In this case, even though the interface of NiO-$SrTiO_3$ appears to be very rough and chemical diffusion is found, no defects such as misfit dislocations can be observed (see the

supplementary material for Figure S1[31]). This could imply that the epitaxial NiO nanocrystals have a different RS mechanism as compared to (the conductive filaments model of) the polycrystalline NiO thin films. The observed oxygen deficiency at the boundary of NiO and $SrTiO_3$ would imply that the interface between the nanocrystals and the substrate could serve as a reservoir or oxygen vacancies. Very likely, this structurally and chemically rough interface can offer the shortest paths for the migration of the oxygen vacancies (which act as minority carriers) to occur. This would explain how the measured RS in NiO nanocrystals is a defect-driven mechanism rather than an intrinsic property of the material itself.[1]

In conclusion, we have characterized the interface structure between RS epitaxial NiO nanocrystals and the underlying $SrTiO_3$ substrate through HAADF-STEM imaging and analysis by EDX and EELS. The interface is physically and chemically rough but without misfit dislocations. There is local chemical disorder evidenced by Ni, Ti, and Sr inter-diffusion. The EELS confirm not only chemical disorder but also a shift in the Ti $L_{2,3}$ peaks and the presence of oxygen vacancies. R × A measurements hint that the RS stems from an interface driven mechanism. The rough interface facilitates a lattice pathway, through which such defects can easily move. As oxygen vacancies have been postulated to control the resistive polarity and conductance in other transition metal oxides, such as TiO_2[40] and perovskites, such as $SrTiO_3$[41] and $Pr_{0.7}Ca_{0.3}MnO_3$,[42,43] we believe this study will motivate further investigations on the role of interface chemistry in such materials.

The research at UNSW was supported by an ARC Discovery and LIEF Grant. The research at Monash Centre for Electron Microscopy (MCEM) used equipment funded by Australian Research Council Grant No. LE0454166 (FEI Titan 80–300 FEGTEM). We thank MCEM, Microscopy Units (EMU) at UNSW and Australian Centre for Microscopy and Microanalysis (ACMM) at USYD for the provision of equipment and technical support. The author would also like to acknowledge Dr. Ye Zhu for his contribution in discussing the results.

[1] J. Sullaphen, K. Bogle, X. Cheng, J. M. Gregg, and N. Valanoor, Appl. Phys. Lett. **100**, 203115 (2012).
[2] R. Powell and W. Spicer, Phys. Rev. B **2**, 2182 (1970).
[3] M. Fraune, U. Rudiger, G. Guntherodt, S. Cardoso, and P. Freitas, Appl. Phys. Lett. **77**, 3815 (2000).
[4] J. Wang, J. Cai, Y.-H. Lin, and C.-W. Nan, Appl. Phys. Lett. **87**, 202501 (2005).
[5] M.-S. Wu and C.-H. Yang, Appl. Phys. Lett. **91**, 033109 (2007).
[6] F. Lin, D. Nordlund, T.-C. Weng, D. Sokaras, K. M. Jones, R. B. Reed, D. T. Gillaspie, D. G. Weir, R. G. Moore, and A. C. Dillon, ACS Appl. Mater. Inter. **5**, 3643 (2013).
[7] M. Z. Sialvi, R. J. Mortimer, G. D. Wilcox, A. M. Teridi, T. S. Varley, K. U. Wijayantha, and C. A. Kirk, ACS Appl. Mater. Inter. **5**, 5675 (2013).
[8] R. Waser and M. Aono, Nat. Mater. **6**, 833 (2007).
[9] M. J. Lee, Y. Park, D. S. Suh, E. H. Lee, S. Seo, D. C. Kim, R. Jung, B. S. Kang, S. E. Ahn, and C. B. Lee, Adv. Mater. **19**, 3919 (2007).
[10] Y.-H. You, B.-S. So, J.-H. Hwang, W. Cho, S. S. Lee, T.-M. Chung, C. G. Kim, and K.-S. An, Appl. Phys. Lett. **89**, 222105 (2006).
[11] J. Son and Y.-H. Shin, Appl. Phys. Lett. **92**, 222106 (2008).
[12] S. I. Kim, J. H. Lee, Y. W. Chang, S. S. Hwang, and K. H. Yoo, Appl. Phys. Lett. **93**, 033503 (2008).
[13] K. Nagashima, T. Yanagida, K. Oka, M. Taniguchi, T. Kawai, J. S. Kim, and B. H. Park, Nano Lett. **10**, 1359 (2010).
[14] J. Y. Son, Y.-H. Shin, H. Kim, and H. M. Jang, ACS Nano **4**, 2655 (2010).
[15] J. Y. Son, C. H. Kim, J. H. Cho, Y.-H. Shin, and H. M. Jang, ACS Nano **4**, 3288 (2010).
[16] C. Lee, B. Kang, A. Benayad, M. Lee, S.-E. Ahn, K. Kim, G. Stefanovich, Y. Park, and I. Yoo, Appl. Phys. Lett. **93**, 042115 (2008).
[17] D.-Y. Cho, S. J. Song, U. K. Kim, K. M. Kim, H.-K. Lee, and C. S. Hwang, J. Mater. Chem. C **1**, 4334 (2013).
[18] M. H. Lee, S. J. Song, K. M. Kim, G. H. Kim, J. Y. Seok, J. H. Yoon, and C. S. Hwang, Appl. Phys. Lett. **97**, 062909 (2010).
[19] K. M. Kim, B. J. Choi, Y. C. Shin, S. Choi, and C. S. Hwang, Appl. Phys. Lett. **91**, 012907 (2007).
[20] H. Shima, F. Takano, H. Muramatsu, H. Akinaga, Y. Tamai, I. H. Inque, and H. Takagi, Appl. Phys. Lett. **93**, 113504 (2008).
[21] M. K. Yang, J.-W. Park, T. K. Ko, and J.-K. Lee, Appl. Phys. Lett. **95**, 042105 (2009).
[22] Y.-C. Chen, Y.-L. Chung, B.-T. Chen, W.-C. Chen, and J.-S. Chen, J. Phys. Chem. C **117**, 5758 (2013).
[23] I. Hwang, M.-J. Lee, G.-H. Buh, J. Bae, J. Choi, J.-S. Kim, S. Hong, Y. S. Kim, I.-S. Byun, and S.-W. Lee, Appl. Phys. Lett. **97**, 052106 (2010).
[24] K. Shibuya, R. Dittmann, S. Mi, and R. Waser, Adv. Mater. **22**, 411 (2010).
[25] J. H. Yoon, J. H. Han, J. S. Jung, W. Jeon, G. H. Kim, S. J. Song, J. Y. Seok, K. J. Yoon, M. H. Lee, and C. S. Hwang, Adv. Mater. **25**, 1987 (2013).
[26] R. Waser, R. Dittmann, G. Staikov, and K. Szot, Adv. Mater. **21**, 2632 (2009).
[27] D. A. Muller, N. Nakagawa, A. Ohtomo, J. L. Grazul, and H. Y. Hwang, Nature (London) **430**, 657 (2004).

[28] R. Klie and N. Browning, Appl. Phys. Lett. **77**, 3737 (2000).
[29] K. A. Bogle, J. Cheung, Y.-L. Chen, S.-C. Liao, C.-H. Lai, Y.-H. Chu, J. M. Gregg, S. B. Ogale, and N. Valanoor, Adv. Funct. Mater. **22**, 5224 (2012).
[30] J. Cheung, M. B. Okatan, J. Sullaphen, X. Cheng, V. Nagarajan, Y.-L. Chen, and Y.-H. Chu, MRS. Commun. **3**, 107 (2013).
[31] See supplementary material at http://dx.doi.org/10.1063/1.4869457 for NiO nanocrystals with various heights and the measured current at pristine/high resistance state are given in Fig. S2.
[32] L. F. Fu, S. J. Welz, N. D. Browning, M. Kurasawa, and P. C. McIntyre, Appl. Phys. Lett. **87**, 262904 (2005).
[33] C. Mitterbauer, G. Kothleitner, W. Grogger, H. Zandbergen, B. Freitag, P. Tiemeijer, and F. Hofer, Ultramicroscopy **96**, 469 (2003).
[34] U. Aschauer, R. Pfenninger, S. M. Selbach, T. Grande, and N. A. Spaldin, Phys. Rev. B **88**, 054111 (2013).
[35] X. Cheng, J. Sullaphen, and N. Valanoor, "Investigation of redox effects at a nanoscale oxide interface" (unpublished).
[36] H. Y. Peng, Y. F. Li, W. N. Lin, Y. Z. Wang, X. Y. Gao, and T. Wu, Sci. Rep. **2**, 442 (2012).
[37] S. Lee, S. Chae, S. Chang, J. Lee, S. Seo, B. Kahng, and T. Noh, Appl. Phys. Lett. **93**, 212105 (2008).
[38] H. Kohlstedt, A. Petraru, K. Szot, A. Rudiger, P. Meuffels, H. Haselier, R. Waser, and V. Nagarajan, Appl. Phys. Lett. **92**, 062907 (2008).
[39] K. Szot, W. Speier, G. Bihlmayer, and R. Waser, Nat. Mater. **5**, 312 (2006).
[40] J. J. Yang, M. D. Pickett, X. Li, D. A. Ohlberg, D. R. Stewart, and R. S. Williams, Nat. Nanotechnol. **3**, 429 (2008).
[41] M. Janousch, G. I. Meijer, U. Staub, B. Delley, S. F. Karg, and B. P. Andreasson, Adv. Mater. **19**, 2232 (2007).
[42] A. Baikalov, Y. Wang, B. Shen, B. Lorenz, S. Tsui, Y. Sun, Y. Xue, and C. Chu, Appl. Phys. Lett. **83**, 957 (2003).
[43] A. Sawa, T. Fujii, M. Kawasaki, and Y. Tokura, Appl. Phys. Lett. **85**, 4073 (2004).